Iraqi National Journal of Earth Science
www.earth.mosuliournals.com

Mineralogical and Geochemical Variations Across the Paleocene-Eocene Sinjar Formation, Dokan Area, Northeastern Iraq

Noor T. Al-Taee [1], Ali I. Al- Juboury [2], Imad M. Ghafor [3]

[1]*Department of Geology, College of Science, University of Mosul, Mosul, Iraq.*
[2]*Department of Petroleum Engineering, College of Engineering, University of Al-Kitab, Kirkuk, Iraq.*
[3]*Department of Geology, College of Science, University of Sulaimani, Sulaimani, Iraq.*

Article information

Received: 00- May -20**

Revised: 00- -June -20**

Accepted: 00- Aug -20**

Available online: 00- Dec – 20**

Keywords:
Paleocene-Eocene
Mineralogy
Geochemistry
Shallow marine
Sinjar Formation

Correspondence:

Name: Noor T. Al-Taee

Email: noortalal@uomosul.edu.iq

ABSTRACT

The Paleocene-Eocene (P-E) Sinjar Formation from Kalka Smaq section, Dokan area, Sulaimaniya, northeastern Iraq has been studied in terms of mineralogy and geochemistry using X-Ray Diffraction (XRD) supported by Scanning Electron Microscopy (SEM) and elemental X-Ray Fluorescence (XRF) geochemical analyses in addition to stable isotopic C and O analysis. The study revealed indications for mineralogical and elemental variation across the P-E transition which may refer to the regionally recognized depositional and paleoclimate changes of the Paleocene Eocene Thermal Maximum (PETM) in the region. The dominance of shallow marine water deposition is interrupted by fresh-water deposition accompanied by increase in temperature suggesting the warming conditions in the Eocene. This result is supported by mineralogical variation in calcite, Mg-calcite and dolomite accompanied with anomalies in $\delta^{18}O$ and $\delta^{13}C$ data and variation in CaO, MgO, SiO_2, TiO_2, Fe_2O_3, and Al_2O_3 in addition to Co, Ni, Sr and Ba elemental data, which in general may suggest the increase in precipitation and low effect of weathering across the P-E transition boundary in the region.

DOI: **********, ©Authors, 20**, College of Science, University of Mosul.

التغاير المعدني والجيوكيميائي عبر الباليوسين–الايوسين في تكوين سنجار، منطقة دوكان، شمال شرقي العراق

نور طلال الطائي[1]، علي إسماعيل الجبوري[2]، عماد محمود غفور[3]

[1]قسم علوم الأرض، كلية العلوم، جامعة الموصل، الموصل، العراق.
[2]قسم هندسة النفط، كلية الهندسة، جامعة الكتاب، كركوك، العراق.
[3]قسم علوم الأرض، كلية العلوم، جامعة السليمانية، السليمانية، العراق.

معلومات الارشفة

تاريخ الاستلام: 00– مايو–**20

تاريخ المراجعة: 00– يونيو–**20

تاريخ القبـول: 00– أغسطس–**20

تاريخ النشر الالكتروني: 00– ديسمبر –**20

الكلمات المفتاحية:
باليوسن – ايوسين
معدنية
جيوكيميائية
البحر الضحل
تكوين سنجار

المراسلة:

الاسم: نور طلال الطائي

Email: noortalal@uomosul.edu.iq

الملخص

لقد تمت دراسة تكوين سنجار (الباليوسين–الايوسين) في مقطع كلكاه سماق، منطقه دوكان، السليمانية، شمال شرقي العراق من الناحية المعدنية والجيوكيميائية باستخدام جهاز حيود الاشعة السينية معززاً بالمجهر الماسح الالكلروني مع التحليل الجيوكيميائي باستخدام جهاز الاشعة السينية الوميضية فضلا عن تحاليل النظائر المستقرة للكاربون والاوكسجين. اظهرت الدراسة دلائلاً للتغاير المعدني والجيوكيميائي عبر تلك الفترة، مما قد يؤشر لما هو مدون عالميا من تغايرات ترسيبية ومناخية قديمة لما يعرف بحدث الحرارة القصوى لفترة الباليوسين–الايوسين. شيوع البيئة البحرية لترسيب عموم التكوين قد انقطع بترسيب حجر جيري في مياه عذبة ومرافقا لتغاير حراري ليؤشر زيادة الحرارة خلال الايوسين. هذه النتيجه عُززت بالتغاير المعدني لوجود الكالسايت والكالسايت الغني بالمغنيسيوم والدولومايت، فضلا عن الشذوذ الواضح بقيم نظيري الاوكسجين والكاربون والتغاير الجيوكيميائي في قيم الاكاسيد الرئيسة من الكالسيوم والمغيسيوم والسليكا والتيتانيوم والحديد والالمنيوم، فضلا عن التغاير في قيم العناصر الشحيحة من الكوبالت والنيكل والسترونتيوم والباريوم ليقترح زياده في الترسيب مع قلة تاثير التجوية للمنطقة خلال تلك الفترة.

DOI: **********, ©Authors, 20**, College of Science, University of Mosul.

Introduction

The Paleocene-Eocene period includes several events that are regionally recognized, such as the Paleocene-Eocene Thermal Maximum (PETM) and the Oceanic Anoxic Events (OAEs) that are characterized by various climatic and paleoenvironmental changes affecting the sedimentary environments and their bio-content due to change in carbon and biochemical cycles (Singh et al., 2022). The Thermal Maximum (~55.5 Ma) represents a period of geologically rapid, extreme global warming, superimposed on a long-term warming trend of the early Cenozoic (Kennett and Stott, 1991; Zachos et al., 2008).

Bowen et al. (2006) considered that rapid and extreme changes in earth system may be triggered by natural carbon cycle perturbation even in times of globally warm climate and in an ice-free world and the PETM phenomena was the obvious indicator to that perturbation.

The Paleocene-Eocene (P-E) boundary is characterized by various biological, mineralogical, and geochemical factors that explain the global paleoenvironmental changes including significant climatic changes. These changes include a strong negative carbon isotope excursion (CIE ranging from −2 to −7‰) as reported by Kender et al. (2012). An increase in water salinity, a decrease in oxygen levels, a shoaling of the Calcite Compensation Depth (CCD), an extinction of approximately 50% of benthic foraminifera, and a turnover in most of the calcareous nannofossils and planktic foraminifera (Gawenda et al., 1999; Zachos et al., 2008; Alegret et al., 2009; Self-Trail et al., 2012; Al-Fattah et al., 2017; Keller et al., 2018; Al-Fattah et al., 2020a; Ghandour, 2020).

In the current study, an outcrop section of Sinjar Formations (late Paleocene-early Eocene) at Kalka Smaq, near Dokan area, northeastern Iraq has been chosen and subjected to mineralogical investigation and geochemical analyses using X-Ray Diffraction (XRD) supported by Scanning Electron Microscopy (SEM), and elemental X-Ray Fluorescence (XRF). The Sinjar Formation is predominantly made up of well-layered limestone, which has undergone recrystallization.

This paper aims to characterize the variations in mineralogical components and geochemical major and trace elements across the P-E boundary in the Sinjar Formation and to determine the possible causes for such variation in relation to the global paleoenvironmental changes during this period.

Geological setting

The study area is located in the Iraqi part of the Western Zagros Fold–Thrust Belt, at the boundary between the High and Low Folded Zones (Jassim and Goff, 2006).

At the end of the Paleocene, the Tethyan Ocean was an extensive northward deepening epicontinental basin covering most of the Arabian Craton including Iraq and neighboring areas. The southern margin of the Tethys was strongly affected by intermittent upwelling episodes due to its location in the northern tropical zone (Speijer and Wagner 2002; Schulte et al., 2011). In the region, multiple stratigraphic sections exhibiting biotic and geochemical evidences associated with upwelling episodes show comparable and unique characteristics that indicate significant global changes during the Paleocene-Eocene period (Almogi-Labin et al., 1993).

The Sinjar Formation is one of the most important formations in the Paleocene-lower Eocene cycle. During this period, shallow-marine carbonates of Sinjar Formation lapped on far onto the Arabian Craton with a maximum flooding (Pg10) being reached in the Early Eocene (Ziegler, 2001). Deposition was characterized by calcarenitic limestones and dolomites dominated by a variety of pelecypods and gastropods and Dasycladaceae (algae), that represent deposition in a protected to lagoonal depositional environment (Fig. 1).

Tectonically, the studied section lies in the northeastern part of the Arabian Plate. According to the tectonic map of Iraq (Fouad, 2015), the Kalka Smaq section lies on Lat. 36°43'31" N and Long. 45°36'27" and is located in the High Folded Zone on the Unstable Shelf of Arabian Plate (Jassim and Goff, 2006) (Fig. 2).

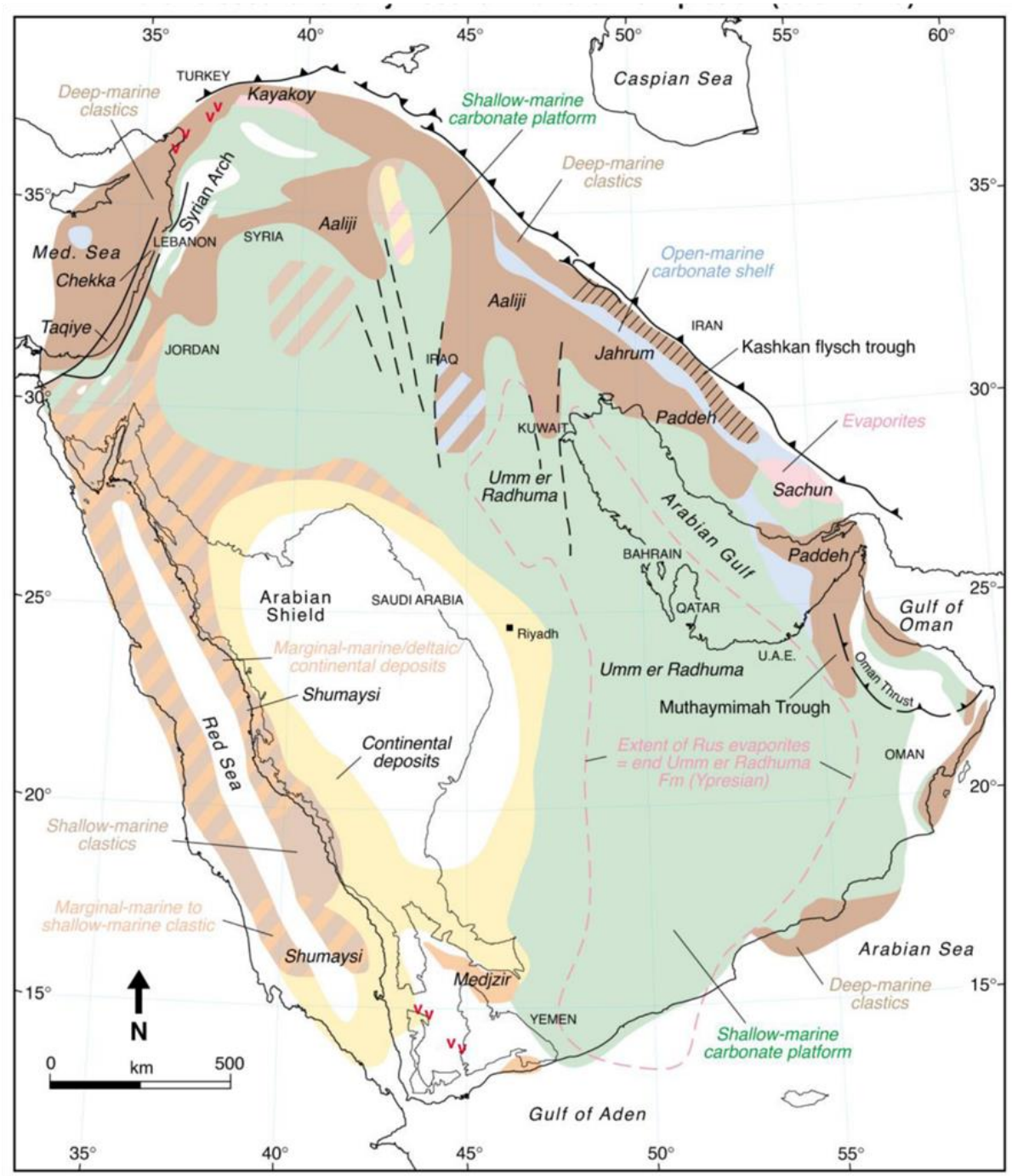

Fig. 1. Late Paleocene to Early Eocene (Thanetian to Ypresian 60.9–49 Ma) paleofacies map (after Ziegler, 2001) illustrating deposition of shallow-marine platform carbonates of Sinjar Formation interfingering with deep-marine clastics and carbonates of the Aaliji Formation.

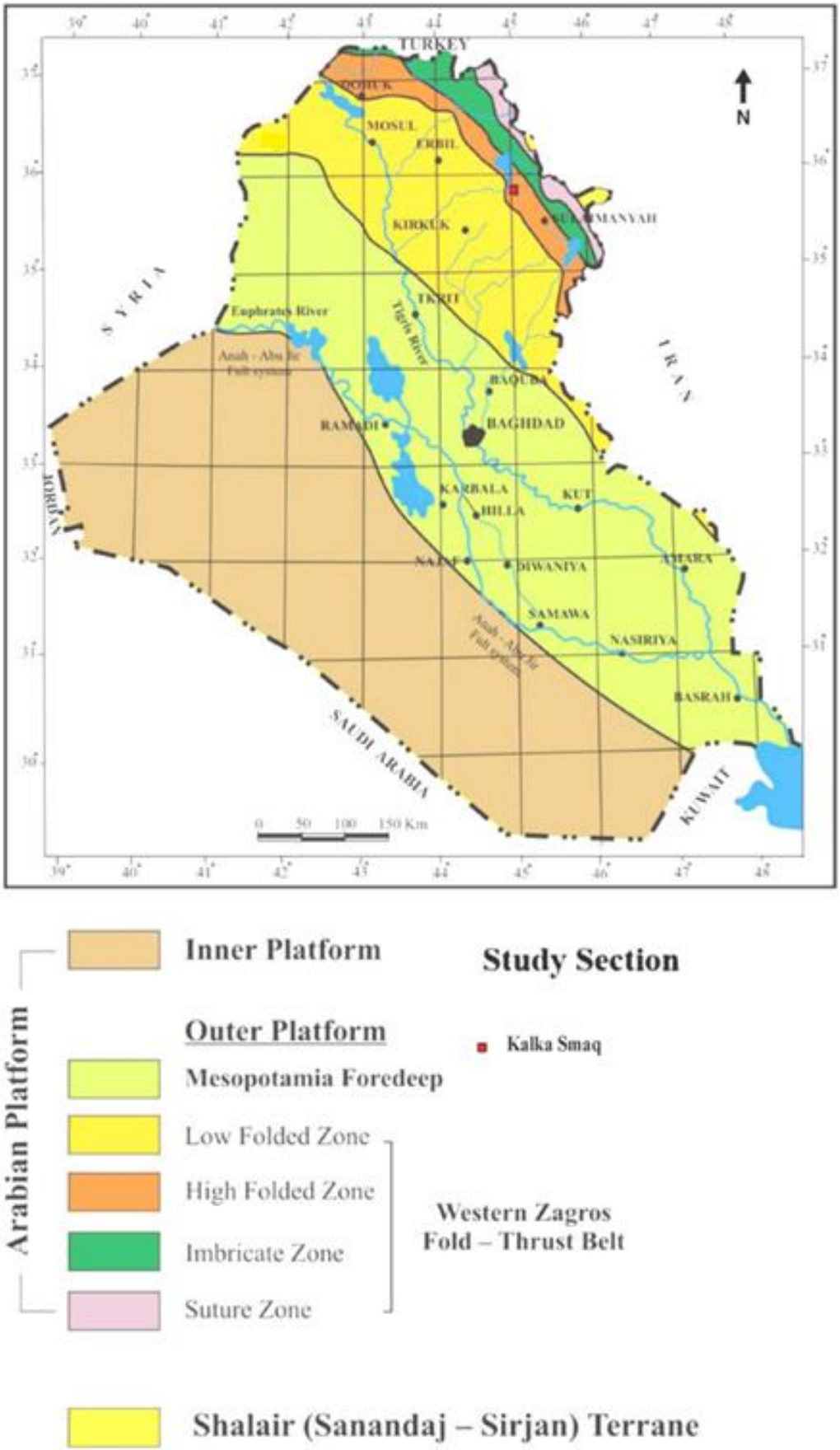

Fig. 2. Tectonic divisions of Iraq (after Fouad, 2015) and the location of the studied sections.

Materials and Methods

Surveying the area and collecting data are the first step for this study. Additionally, field trips are conducted to obtain more informations and accurate data about the studied area. Totally, 125 rock samples are collected and subjected to various required analyses.

X-Ray diffraction (XRD) mineralogy analysis is performed on the selected bulk, whole rock samples at Premier Corex Laboratories in Houston, U.S.A. using a Bruker D8 Advance XRD instrument equipped with a theta-theta goniometer with a 250 cm radius and a Lynxeye XE-T detector. All measurements are performed using CuK radiation, and the applied voltage and current are 40 kV and 30 mA respectively. Quantification of mineral phases in the bulk diffraction pattern is accomplished using the TOPAS software package.

Scanning electron microscopy (SEM) analysis is completed on selected samples at Premier Corex Laboratories in Houston, U.S.A. using an FEI Quanta FEG 650 FE-SEM instrument equipped with two Bruker EDS XFlash 5030 energy dispersive X-ray spectroscopy (EDS) detectors and an FEI R580 Everhart-Thornley (ETD) electron detector.

The XRF analysis is done on the selected bulk, whole rock samples using a Bruker Tracer 5i XRF instrument installed at Premier Corex Laboratories in Houston, U.S.A.

Stable isotopic analysis of $\delta^{13}C$ and $\delta^{18}O$ are measured using an automated carbonate preparation device (KIEL-III) and a Finnegan MAT 252 isotope ratio mass spectrometer at the Environmental Isotope Laboratory, University of Arizona, USA.

Results

Mineralogy

The mineralogical compositions of carbonate samples at the Kalka Smaq section determined by X-ray diffraction reveal calcite, Mg-calcite, dolomite and Fe-dolomite as the main mineralogical components, in addition to less quartz and clay minerals (smectite and illite mica with traces of chlorite, palygorskite and serpentine) (Table 1). The X-ray diffractograms of the selected bulk, whole rock carbonate samples across the P-E boundary are illustrated in Figure (3), while the selected scanning electron micrographs for the main components of the studied samples are shown in Figure (4).

It is worth to mention that biostratigraphic study of the studied section has revealed that the studied samples are taken across Paleocene–Eocene (P-E) boundary, where samples 58-90 represent the Paleocene (Thanetian), while samples 100-119 are taken from the Eocene (Ypresian) (Al-Taee, et al., 2023) (Table 1).

Calcite and Mg-calcite form the main and abundant minerals along the studied section with higher amount (62%) calcite in sample 113, which may represent the transition boundary from the Paleocene to Eocene. This is supported by abrupt change in stable isotopic carbon and oxygen data as represented by a strong negative carbon isotope excursion (CIE −9.99‰) , (Table 2, Fig. 5) and increased amount of quartz, illite and chlorite, while the values of Mg-calcite, dolomite and Fe-dolomite show the lesser amounts in this sample (Table 1). The CIE recovery phases show a decrease in calcite and Mg-calcite, while dolomite and Fe-dolomite increase, this is accompanied with increase in quartz and smectite ratios (Table 1, Fig. 4).

The morphological phases of the carbonate minerals as deduced from the SEM study include the star-shaped form of the Mg-calcite, columnar and anhedral calcite crystals, dolomite rhombs, palygorskite fibers and fine rhombohedra authigenic calcite mineral (Fig. 4).

Table 1: Mineralogical components of the main framework and clay minerals composition as revealed from XRD study. Samples from 58-90 represent the Paleocene rocks, while those from 100-119 represent the Eocene rocks.

Sample	Main components						Clay Minerals					
	Qz %	Clays &	Calcite %	Mg-Calcite %	Dolomite %	Fe-Dolomite %	Smectite %	Illite+ Mica%	Chlorite %	Palygorskite %	Serpentine %	Total %
119	5.6	2.5	1.7	4.2	74.6	11.0	1.6	0.3	0.2	0.0	0.4	2.5
113	5.4	1.9	62.1	30.3	Trace	0.3	0.5	0.8	0.6	0.0	0.0	1.9
110	0.9	0.6	20.4	69.6	2.5	6.0	0.6	0.0	0.0	0.0	0.0	0.6
108	1.8	0.8	19.4	77.5	0.2	0.3	0.8	0.0	0.0	0.0	0.0	0.8
100	2.9	0.6	13.8	82.4	Trace	0.3	0.6	0.0	0.0	0.0	Trace	0.6
90	1.0	0.6	26.8	70.6	0.4	0.6	0.6	0.0	0.0	0.0	0.0	0.6
80	1.0	0.6	15.5	81.0	0.5	1.4	0.6	0.0	0.0	Trace	Trace	0.6
71	1.3	3.7	13.4	80.0	0.4	1.2	0.8	0.0	0.0	2.7	0.2	3.7
66	1.4	0.8	10.4	83.2	1.0	3.0	0.6	0.0	0.0	0.0	0.2	0.8
58	4.2	3.5	18.0	40.0	20.0	12.5	1.6	0.0	0.4	1.5	Trace	3.5

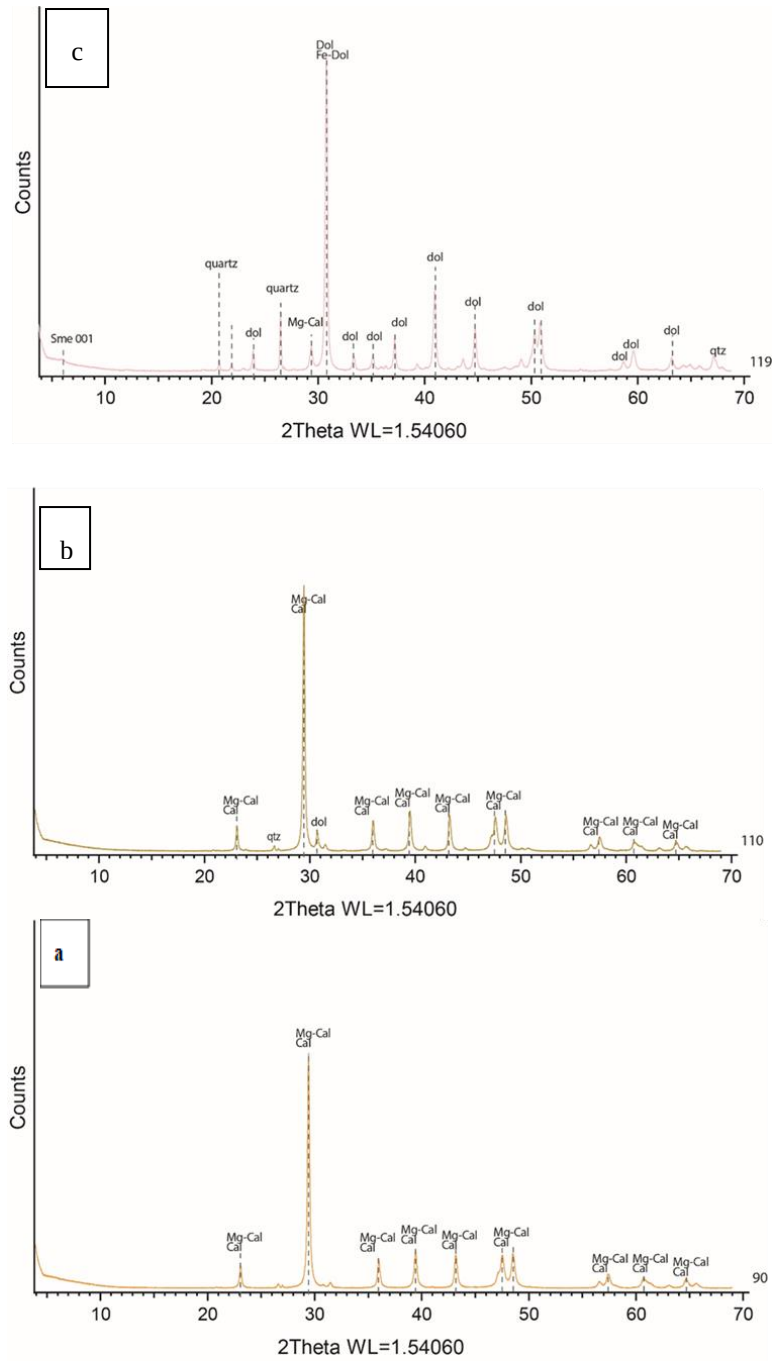

Fig. 3. X-ray diffractograms of selected bulk whole-rock samples from Sinjar Formation showing the main mineralogical components (samples, a-90, b- 110 and c- 119)

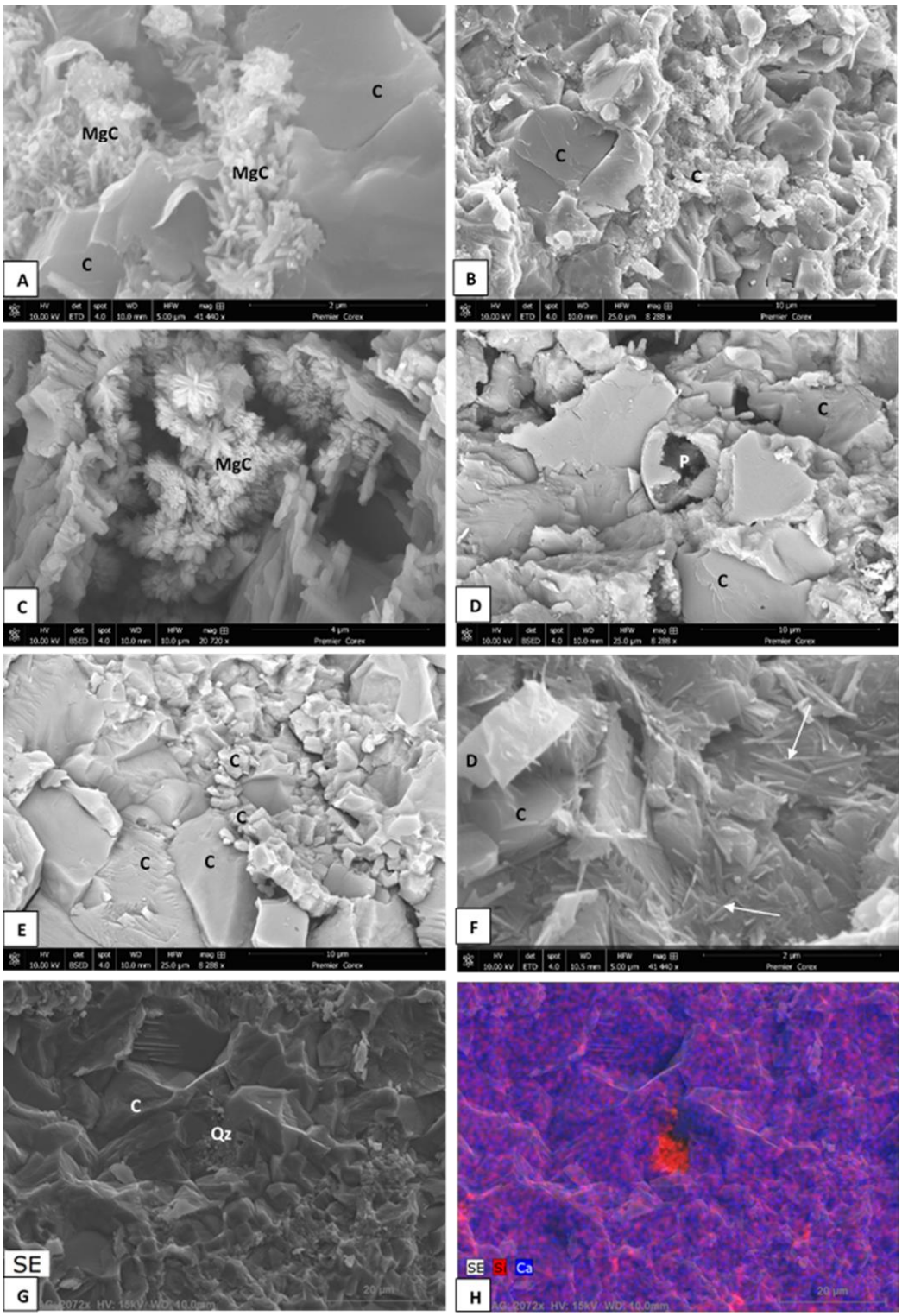

Fig. 4. SEM micro images of selected samples from Sinjar Formation showing; A- Main Mg-calcite (MgC) in star-shapes and calcite sub-columnar and anhedral shapes (C), sample 113. B- Fine grained and coarse-grained calcite (C) due to recrystallization, sample 113. C- Rose-shaped Mg-calcite in the center of the view, sample 100, D- Common calcite anhedral grains (C) with dissolution forming pores (P), sample 100. E- Recrystallization, the common diagenetic process in the Sinjar Formation, fine to coarse crystals of calcite (C), sample 80. F- Palygorskite fibers (arrows) with dolomite (D) and calcite (C), sample 71. G- quartz authigenesis (Qz) in rhombohedra forms and calcite (C) in sample 71. H- same sample under energy dispersive X-ray spectroscopy (EDS) showing the quartz (Si) within main carbonate (Ca) elemental composition.

Geochemistry

Stable isotopic data

The $\delta^{13}C$ values vary from -9.99 ‰, to 3.69 ‰ VPDB, some of the samples record negative values particularly in the suggested Eocene samples whilst others have positive values (Table 2, Fig. 4). The $\delta^{13}C$ (VPDB) values for marine carbonate rocks are usually constant and close to zero, while on the other hand, fresh-water limestones are usually enriched in $\delta^{13}C$ as a result of the organic influences (Moore, 2001; Adelabu et al., 2021). The strong negative value is recorded in sample 113, which is suggested as mentioned earlier to represent the boundary between the Paleocene and Eocene periods in the limestone of the Sinjar Formation.

Table 2: $\delta^{13}C$ and $\delta^{18}O$ values of the Sinjar limestone from Kalka Smaq section, samples from 58-95 represent the Paleocene rocks while those from 100-120 represent the Eocene rocks.

Sample No.	δ 13C (‰VPDB)	δ 18O (‰VPDB)	Temperature °C T	Environment Z
S120	-0.53	-5.18	42.5	123.6
S119	-0.01	-1.61	24.2	126.5
S117	0.58	-1.52	23.8	127.7
S113	-9.99	-5.99	47.0	103.8
S112	2.66	-5.05	41.8	130.2
S110	3.28	-4.76	40.2	131.6
S108	1.43	-5.36	43.5	127.6
S100	-0.82	-5.32	43.3	122.9
S95	2.99	-4.19	37.2	131.3
S90	2.40	-4.99	41.4	129.7
S85	2.84	-3.47	33.4	131.4
S84	3.69	-1.05	21.6	134.3
S80	2.22	-4.12	36.8	129.8
S77	0.66	-3.61	34.2	126.8
S71	1.75	-4.61	39.4	128.6
S66	2.60	-4.74	40.1	130.2
S63	2.14	-2.70	29.5	130.3
S58	0.60	-3.54	33.8	126.9
S52	-1.86	0.52	14.6	123.7
S46	-0.33	-0.03	17.0	126.6

In this study, $\delta^{18}O$ values range from -0.03‰ to -5.99‰ VPDB (with exception of sample 52 which is 0.52‰ VPDB). The strong negative value also is recorded from sample 113 (Table 2, Fig. 4).

Using the $\delta^{18}O$ and $\delta^{13}C$ data of the studied Sinjar Formation to deduce the depositional environment and paleotemperature, the following equations (1 and 2) are applied. For the best discriminations between marine and freshwater limestones, equation (1) of Keith and Weber (1964) is used:

$$Z = a\,(\delta^{13}C + 50) + b\,(\delta^{18}O + 50) \quad \text{..... (1)}$$

Where, a = 2.048, b =0.498, $\delta^{18}O$ = Oxygen isotopic composition of the limestone (vPDB). $\delta^{13}C$ = Carbon isotopic composition of limestone (vPDB).

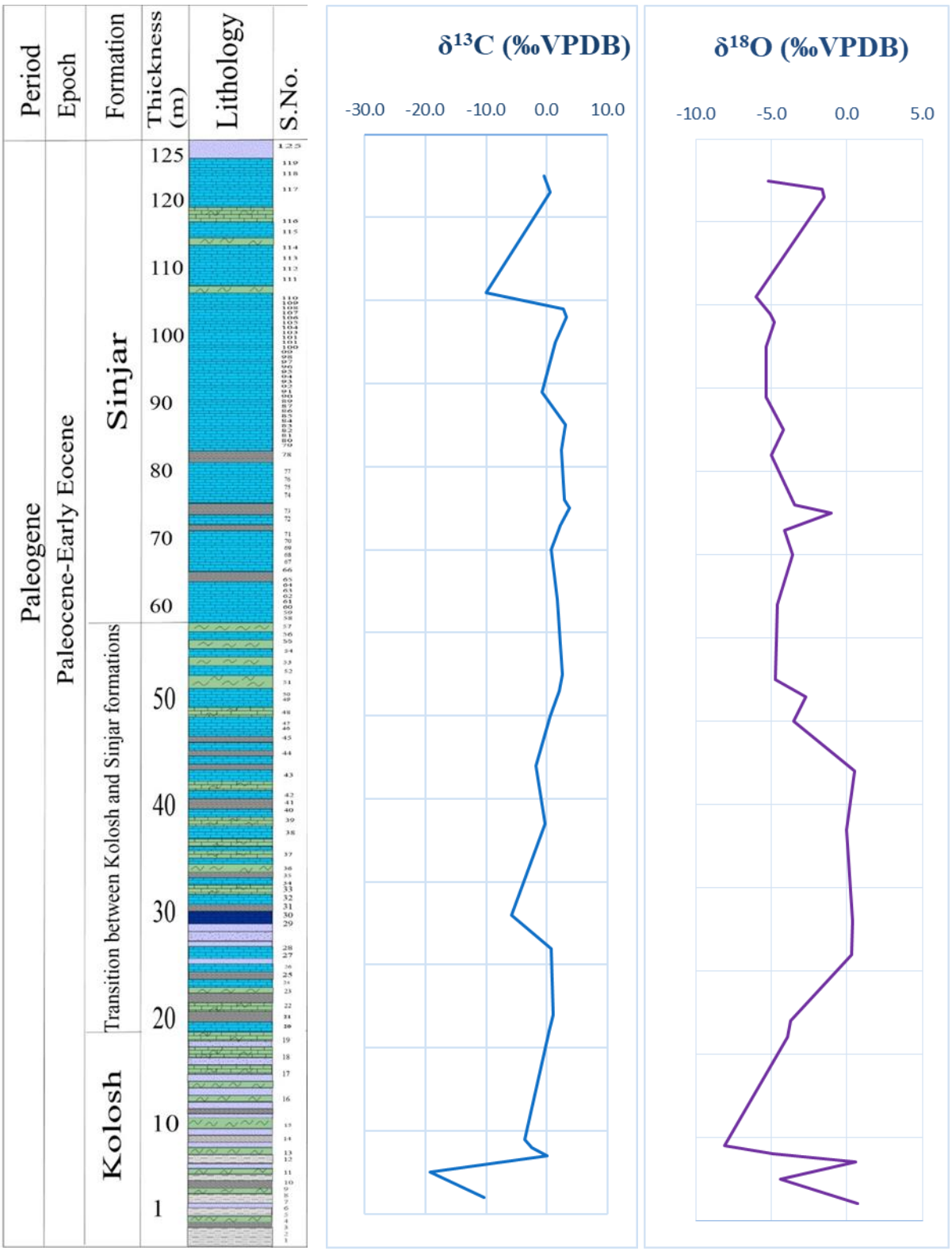

Fig. 5. Vertical distribution of δ13C and δ18O values along the Sinjar and the upper part of the transition zone between the Sinjar and Kolosh Formations at Kalka Smaq section.

Limestone samples with a (Z) value above 120 would be classified as marine, while those with (Z) values below 120 as fresh-water limestone.

The studied Paleocene-Eocene Sinjar limestone samples in the study area are classified into marine limestone with calculated (Z) values ranging from 122.9 to 134.3, except sample 113, which represents fresh-water environment with (Z) value of 103.8 (Table 2).

While the estimated paleo temperature values for the studied limestone ranging from 17 °C to 47 °C (Table 2) is inferred using Equation (2) (Shackleton and Kennett, 1975).

$$T = 16.9 - 4.38(\delta c^{18}O - \delta w^{18}O) + 0.1(\delta c^{18}O - \delta w^{18}O)2 \quad \text{..... (2)}$$

Where, $\delta c^{18}O$ = Oxygen isotopic composition of limestone (vPDB). $\delta w^{18}O$ =Oxygen isotopic composition of seawater (vsMOW), (which is assumed to be $dw^{18}O = \delta^{18}O$ ($_{VS}$MOW) -1.00%; (Shackleton and Kennett, 1975; Kim et al., 2015).

This equation is an expression of the isotopic equilibrium between water and calcite.

Major and trace elements data

Distribution of the major and trace elements in the Paleocene and Eocene carbonate rocks are illustrated in Table (3).

CaO and MgO form the main oxides along the studied section. CaO% ranges from 34.48 to 52.81% in the studied Paleocene limestones, whereas, it ranges between 26.34 to 53.08% in the Eocene limestone with abrupt decrease in the upper part of the section (samples 117-120). In contrast, these samples show higher MgO values (Table 3), whereas MgO ranges between 1.07 to 11.89% in the Paleocene limestones, and from 1.02 to 18.76% in the Eocene limestones.

It is worth to mention that these uppermost samples of the studied section contain higher amounts of SiO_2, Al_2O_3, Fe_2O_3, Na_2O, K_2O and the trace elements of V, Co and Ni, while Sr and Ba values are less.

Discussion

Mineralogical and geochemical variation across the Paleocene-Eocene Sinjar limestones from Kalka Smaq section, Dokan area, northeastern Iraq has revealed several indications to the depositional and paleoclimate changes from Paleocene to Eocene including the PETM event that have affected on the distribution of mineralogical and elemental composition.

The overall deposition was occurring in marine setting as revealed from the stable isotopic data. Previous studies on the depositional environment of the Sinjar Formation have mentioned a shallow marine fore reef (shoal) deposition (Al-Qayim et al., 1993; Al-Haj, 2001; Amin, et al., 2005). The presence of coarse-grained calcite and fine-grained micritic grains as revealed from the SEM study may indicate the high energy and low energy conditions in depositional environment.

Dominance of Mg-calcite over calcite and other carbonate minerals support deposition in shallow marine saline water similar to present-day depositional environments of shallow carbonates, e.g. Bahamas, Florida shelf, Arabian Gulf, Yucatan, and Red Sea (Wilson, 1997).

The anomaly of the increase in calcite and decrease in Mg-calcite is recorded from sample 113, which also have the strong negative carbon and oxygen isotopes excursion accompanied by increased amount of quartz, illite and chlorite (Tables 1 and 2). This sample was deposited in fresh-water carbonate and may represent the PETM period and the Paleocene-Eocene boundary at the studied section. Generally, the more negative values of δ18O in Eocene limestones of the study area (Table 2) reflect increasing temperature than those from the Paleocene (Scott et al., 2013, Al-Fattah et al., 2020b).

The presence of illite in the uppermost part of the succession may refer to increase of dry climate accompanied with increase in dolomite (see sample 119, Table 1), this mineralogical association also refers to closed dry conditions favorable to deposition of dolomite, gypsum,

smectite and illite (Chamley, 1989) and may represent lagoonal dry periods in the deposition of the Sinjar Formation.

The geochemical data support the results of increasing amount of Mg content in the uppermost samples of the studied succession and supporting the dolomite deposition where Mg/Ca ratio was favorable to this deposition. This is also accompanied by increase in SiO_2, TiO_2, Fe_2O_3, and Al_2O_3 contents that are suitable in more weathering conditions affecting this area after warming condition at the P-E transition (Chen et al., 2016; Enneili et al., 2019).

All the above data may refer to increase of precipitation associated with the Paleocene-Eocene transition and the PETM warming in the studied section of the Sinjar Formation.

Table 3: Major oxides (wt.%) and selected trace elements (ppm) data for limestone and marly limestone, Kalka Smaq section. Samples from 58-95 represent the Paleocene rocks while those from 100-120 represent the Eocene rocks.

Sample	SiO_2 %	TiO_2 %	$Al2O_3$ %	Fe_2O_3 %	MnO %	MgO %	CaO %	Na_2O %	K2O %	P_2O_5 %	SO_3 %	V ppm	Cr ppm	Co ppm	Ni ppm	Cu ppm	Zn ppm	Rb ppm	Sr ppm	Mo ppm	Ba ppm	Th ppm	U ppm
S120	2.55	0.03	0.20	2.02	0.04	15.43	34.63	0.61	0.14	0.06	0.17	220	18	12	82	25	10	0	122	1	35	2	2
S119	8.63	0.07	0.36	2.83	0.05	17.90	26.82	0.48	0.13	0.07	0.14	294	16	17	110	18	12	0	56	0	52	2	2
S117	5.32	0.08	0.75	3.60	0.04	18.76	26.34	0.71	0.23	0.07	0.17	306	23	16	74	13	20	1	65	1	86	2	2
S113	6.93	0.02	0.88	1.42	0.03	1.02	48.31	0.15	0.15	0.07	0.16	21	32	24	224	40	21	2	43	3	0	1	2
S112	0.62	0.00	0.13	0.35	0.03	0.97	53.08	0.10	0.13	0.05	0.14	0	19	1	45	22	9	2	323	6	13	1	2
S110	0.63	0.01	0.12	0.42	0.03	1.93	50.04	0.14	0.14	0.05	0.15	7	19	2	46	16	8	0	345	14	21	1	4
S108	2.41	0.01	0.42	1.08	0.03	1.44	50.42	0.17	0.14	0.04	0.14	17	25	9	76	19	13	0	141	6	0	1	3
S100	1.72	0.01	0.22	0.53	0.03	1.15	51.66	0.12	0.15	0.05	0.14	0	21	3	44	14	9	0	216	1	24	1	5
S95	1.80	0.02	0.32	0.78	0.03	2.48	47.86	0.15	0.14	0.06	0.17	30	22	5	70	14	12	2	239	10	41	1	3
S90	0.56	0.00	0.13	0.33	0.03	1.07	52.81	0.11	0.13	0.04	0.14	0	18	1	42	16	8	1	241	7	3	1	3
S85	2.38	0.02	0.27	1.21	0.03	6.31	38.68	0.25	0.15	0.05	0.19	112	25	7	65	23	13	0	267	5	11	1	4
S84	0.71	0.00	0.16	0.46	0.03	1.11	52.66	0.10	0.13	0.05	0.15	0	18	2	53	13	9	0	225	4	10	1	2
S80	0.81	0.01	0.19	0.47	0.03	1.34	51.86	0.11	0.15	0.05	0.19	0	19	2	49	19	12	0	216	5	33	1	2
S77	4.22	0.01	0.45	1.18	0.02	1.80	48.05	0.22	0.21	0.06	0.59	34	25	10	82	28	15	6	312	13	9	1	6
S71	2.64	0.01	0.43	0.63	0.03	1.73	49.27	0.15	0.19	0.06	0.28	25	23	5	79	17	10	1	358	8	38	1	4
S66	1.38	0.00	0.26	0.56	0.03	1.68	50.54	0.11	0.14	0.05	0.26	6	19	3	49	17	11	0	281	8	13	1	3
S63	3.28	0.04	0.52	1.57	0.03	11.89	39.07	0.34	0.18	0.05	0.21	189	26	9	80	16	13	0	324	2	56	1	3
S58	7.75	0.05	0.93	1.93	0.02	6.86	34.48	0.35	0.28	0.07	1.26	115	26	15	91	24	17	6	203	4	96	2	2

Conclusions

The study of the mineralogical and geochemical variation across the Paleocene-Eocene transition in Sinjar limestones from Kalka Smaq section, Dokan area, northeastern Iraq has revealed several indications for mineralogical and elemental variation across the P-E accompanied with the regionally recognized depositional and paleoclimate changes of the Paleocene Eocene Thermal Maximum PETM. The shallow marine water deposition is interrupted by fresh-water deposition accompanied by increase in temperature suggesting the warming conditions in the Eocene. Variation in Mg-calcite, calcite and dolomite and presence of some clay minerals of smectite and illite supported by anomalies in $\delta^{18}O$ and $\delta^{13}C$ data and variation in CaO, MgO, SiO_2, TiO_2, Fe_2O_3, and Al_2O_3 in addition to Co, Ni, Sr and Ba elemental data may suggest the increase in precipitation and low effect of weathering across the P-E transition boundary in the region and giving an indication of warming condition during the P-E transition in the region.

References

Adelabu, I.O., Opeloye, S.A. and Oluwajana, O.A., 2021. Petrography and geochemistry of Paleocene-Eocene (Ewekoro) limestone, eastern Benin basin, Nigeria: implications on depositional environment and post-depositional overprint. Heliyon Vol.7, pp. 1-12. DOI: 10.1016/j.heliyon. 2021.e08579

Alegret, L., Ortiz, S., Orue-Etxebarria, X., Bernaola, G., Baceta, J. I., Monechi, S., et al., 2009. The Paleocene–Eocene thermal maximum: new data on microfossil turnover at the Zumaia section, Spain. Palaios, Vol. 24, pp.318–328. DOI: 10.2110/palo. 2008.p08-057r

Al-Fattah, A.N., Al-Juboury, A.I., Ghafor, I.M., 2017. Paleocene-Eocene Thermal Maximum (PETM) of Northern Iraq, Lambert Academic Publishing, Mauritius, pp. 212

Al-Fattah, A.N., Al-Juboury, A.I., Ghafor, I.M., 2020a. Significance of Foraminifera during the Paleocene-Eocene Thermal Maximum (RETM) in the Aaliji and Kolosh Formations. Iraqi Bulletin of Geology and Mining, 16(2), 33–50.

Al-Fattah, A.N., Al-Juboury, A.I., Ghafor, I.M., 2020b. Paleocene-Eocene Thermal Maximum Record of Northern Iraq: Multidisciplinary Indicators and an Environmental Scenario. Jordan Journal of Earth and Environmental Sciences,11(2), 126-145.

Al-Haj, M.A.M., 2001. Sedimentary model of the Sinjar Formation from northwestern Iraq. Unpublished M.Sc. thesis, Mosul University, pp. 141 (In Arabic)

Almogi-Labin, A., Beim, A., Sass, E., 1993. Late Cretaceous upwelling system along the southern Tethys margin (Israel): interrelationship between productivity, bottom water environments and organic matter preservation. Paleoceanography, Vol.8, pp. 671–690. DOI:10.1029/93PA02197

Al-Qayim, B., Al-Shaibani, Sh. Nisan, B., 1993. Stratigraphic Evolution of Paleogene Sequence, Haibat-Sultan, Northeastern Iraq, Jour. Geol. Soc. Iraq, 21(2), 55–66.

Al-Taee, N.T., Ghafor, I.M., Al-Juboury, A.I., Dettman, D.L., 2023. Biostratigraphy and paleoecology of the Sinjar Formation (Late Paleocene-Early Eocene) in Dokan and Sinjar areas, Iraq, Iraqi Geological Journal Vol. 57 (1A), pp. 221-249.

Amin, M.A., Al-Mutwali, M. M., Thannon, T. A., 2005. Microfacies and paleoenvironment of Sinjar Formation (Paleocene – Early Eocene), Sinjar Area. Rafidain Jour Science, Special issue,Vol. 16, pp.1–20. DOI: 10.33899/rjs.2005.41386

Bowen, G. J., Bralower, T. J., Delaney, M. L., Dickens, G. R., Kelly, D. C., Koch, P. L., Kump, L. R., Meng, J., Sloan, L. C., Thomas, E., Wing, S. L., Zachos, J. C., 2006. Eocene hyperthermal event offers insight into greenhouse warming. Eos, Transactions of the American Geophysical Union, 87(17), 165–169. https://doi.org/10.1029/2006eo170002

Chamley, H., 1989. Clay Sedimentology. Springer-Verlag, Berlin, pp. 623.

Chen, Z., Ding, Z., Yang, S., Zhang, C. and Wang, X., 2016. Increased precipitation and weathering across the Paleocene-Eocene Thermal Maximum in central China. Geochemistry, Geophysics, Geosystem, AGU Publications, American Geophysical Union, pp.2286-2297. https://doi.org/10.1002/2016GC006333

Enneili, A., Amel, H.A., Felhi, M. Zayani, K., Fattah, N. and Tlili, A., 2016. Geochemistry and mineralogy of Plaeocene-Eocene depositional sequence in Oued Thelja Section, SW Gafsa, Tunisia. In: Doronzo, D.M. et al., (eds.). Petrogenesis and Exploration of the Earth's Interior, Springer Nature Switzerland AG., pp.121-124. DOI: 10.1007/978-3-030-01575-6_29

Fouad, S.F.A., 2015. Tectonic Map of Iraq, SCALE 1:000 000, 3rd Edition, 2012. Iraqi Bulletin of Geology and Mining, 11(1),1–8.

Gawenda, P., Winkler, W., Schmitz, B., et al. ,1999. Climate and bioproductivity control on carbonate turbidite sedimentation (Paleocene to earliest Eocene, Gulf of Biscay, Zumaia, Spain). Journal of Sedimentary Research, 69(6), 1253–1261. DOI: 10.2110/jsr.69.1253

Ghandour, I.M., 2020. Paleoenvironmental changes across the Paleocene–Eocene boundary in West Central Sinai, Egypt: geochemical proxies. Swiss J Geoscience, 113:3, https://doi.org/10.1186/s00015-020-00357-3.

Jassim, S.Z., Goff, J.C., 2006. Geology of Iraq. - Dolin, Prague and Moravian Museum, Brno, pp. 341.

Keller, G., Mateo, P., Punekar, J., et al., 2018. Environmental changes during the Cretaceous-Paleogene mass extinction and Paleocene–Eocene thermal maximum: implications for the Anthropocene. Gondwana Research, Vol.56, pp.69–89. https://doi.org/10.1016/j.gr.2017.12.002

Keith, M.L., Weber, Y.N., 1964. Carbon and oxygen isotopic composition of selected limestone and fossils. Geochem. Cosmochim. Acta 28, pp. 1787–1816.

Kender, S., Stephenson, M. H., Riding, J. B., et al. 2012. Marine and terrestrial environmental changes in NW Europe preceding carbon release at the Paleocene–Eocene transition. Earth and Planetary Science Letters, 353–354, pp.108–120. https://doi.org/10.1016/j.epsl.2012.08.011

Kennett, J. P. and L. C. Stott, 1991. Abrupt deep-sea warming, palaeoceanographic changes and benthic extinctions at the end of the Palaeocene, Nature, Vol. 353, pp. 225–229.

Kim, S.T., Coplen, T.B., Horita, J., 2015. Normalization of stable isotope data for carbonate minerals: implementation of IUPAC guidelines. Geochem. Cosmochim. Acta 158, pp.276–289.

Moore, C.H., 2001. Carbonate Reservoirs: Porosity Evolution and Diagenesis in A Sequence Stratigraphic Framework. Developments in Sedimentology. Elsevier, Amsterdam, p. 444.

Shackleton, N.J., Kennett, J.P., 1975. Paleotemperature History of the Cenozoic and the Initiation of Antarctic Glaciation: Oxygen and Carbon Isotope Analyses in DSDP Sites 277, 279 and 281: Initial Reports of Deep-Sea Drilling Project, 29. U.S. Government Printing Office, Washington, pp. 743–752.

Schulte, P., Scheibner, C., Speijer, R. P., 2011. Fluvial discharge and sea-level changes controlling black shale deposition during the Paleocene– Eocene thermal maximum in the Dababiya Quarry section, Egypt. Chemical Geology, Vol.285, pp.167–183. DOI: 10.1016/j.chemgeo.2011.04.004

Scott, R.W., Formolo, M., Rush, N., Owens, J.D., Oboh-Ikuenobe, F., 2013. Upper Albian OAE 1d event in the Chihuahua Trough, New Mexico, U.S.A Cretaceous Research, Vol. 46, pp.136–150. http://dx.doi.org/10.1016/j.cretres.2013.08.011

Self-Trail, J. M., Powars, D. S., Watkins, D. K., et al. 2012. Calcareous nannofossil assemblage changes across the Paleocene–Eocene thermal maximum: evidence from a shelf setting. Marine Micropaleontology, 92–93, 61–80.

Singh, B., Singh, S. and Bhan, U., 2022. Oceanic anoxic events in the Earth's geological history and signature of such event in the Paleocene-Eocene Himalayan foreland basin sediment records of NW Himalaya, India. Arabian Journal of Geosciences, 15: 317, https://doi.org/10.1007/s12517-021-09180-y

Wilson, J.L., 1997. Carbonate Depositional Environments and Diagenesis, Chapter 2, In: Palaz, I. and Marfurt, K.J. (eds), Carbonate Seismology, Geophysical Development Series, Society of Exploration Geophysicists.

Zachos, J. C., Dickens, G. R., Zeebe, R. E., 2008. An early Cenozoic perspective on greenhouse warming and carbon-cycle dynamics. Nature, Vol. 451, pp.279–283. DOI: 10.1038/nature06588

Ziegler, M.A., 2001. Late Permian to Holocene paleofacies evolution of the Arabian Plate and its hydrocarbon occurrences, GeoArabia, 6(3),445–504. https://doi.org/10.2113/geoarabia0603445